PHYSICAL REVIEW A, VOLUME 65, 030501(R)

Detailed spectroscopy of the $a(1)$ $[^3\Sigma^+]$ state of PbO

L. R. Hunter, S. E. Maxwell, K. A. Ulmer, N. D. Charney, S. K. Peck, D. Krause, Jr., and S. Ter-Avetisyan*
Physics Department, Amherst College, Amherst, Massachusetts 01002

D. DeMille
Physics Department, Yale University, New Haven, Connecticut 06520
(Received 2 November 2001; published 13 February 2002)

An experimental search for the electron electric-dipole moment using the $a(1)[^3\Sigma^+]$ state of PbO is currently underway and promises to yield high precision. Several experimental parameters are required as input to theoretical determinations of the sensitivity of the proposed experiment. We use molecular-beam spectroscopy to determine the hyperfine constant, molecular dipole moment, and Lande g factor of the $a(1)$ state, and the electronic isotope shifts of the X-a transition.

DOI: 10.1103/PhysRevA.65.030501 PACS number(s): 33.20.−t, 33.15.−e, 33.20.Kf, 14.60.Cd

The existence of a permanent electric-dipole moment (EDM) of a fundamental particle violates both parity and time-reversal symmetries. Experimental methods to determine the electron EDM (d_e) have been refined over the last several decades, culminating in the current upper bound: $|d_e|<1.6\times10^{-27}$ e cm [1]. Recently, an EDM experiment was proposed on the $a(1)[^3\Sigma^+]$ state of PbO that may permit measurement of d_e with several orders of magnitude greater precision [2]. If successful, this experiment will have important implications for nearly all extensions of particle physics beyond the standard model, especially supersymmetry.

Challenging molecular theory is required to relate d_e to the measured EDM of the $a(1)$ state. *Ab initio* calculations in heavy molecular systems are notoriously difficult, and must be checked against experimental data on closely related physical quantities. Semiempirical calculations may be easier to perform, but these require the measurement of several parameters (such as hyperfine structure and Lande g factors) [3] that have not been previously determined for the $a(1)$ state. We describe here the determination of several parameters that we expect to provide critical input data for a semiempirical model [4] and constraints on planned *ab initio* calculations [5].

The molecular-beam apparatus used in these experiments is similar to that described in Ref. [2]. A few modifications have been made in order to increase the usable flux and extend the operation time after filling the oven. The new oven has a 99.8% pure alumina liner and a larger volume that is typically loaded with about 30 g of PbO. The oven aperture now has a 0.317 in. diameter and is filled with small-diameter thin-walled tubes to precollimate the beam. The tubes are overheated in order to avoid clogging. In our early measurements, the tubes were 316 stainless steel. These were attacked by PbO and typically required replacement after a few fills of the oven. In our more recent measurements, the tubes are alumina. We now achieve high beam fluxes for many days of operation without depletion of the source. The ceramics show no sign of corrosion or attack by PbO.

In all of our measurements, a 628-nm external- (Littman) cavity diode laser (Sacher Lasertechnik TEC 500) is used to excite specific rotational states from the second vibrational level ($v''=2$) of the ground electronic state $X(0)[^1\Sigma^+]$ to the $a(1)$, ($v'=3$) level. The laser power, while stable for a particular measurement, varies from 2–10 mW over the course of the various measurements. The time-averaged linewidth over 10 s (our integration time between laser-frequency steps) is typically below the residual Doppler broadening of about 25 MHz. Because of the weak nature of the forbidden spin-flip transition, the laser beam has to be passed through the molecular beam many times in order to obtain a reasonable signal-to-noise ratio. This multipass is accomplished by bouncing the laser beam between two flat dielectric mirrors. A 2-in.-diameter mirror is fixed with its reflective surface in vacuum. The opposing vacuum entry window is antireflection coated and a second mirror (of 1 in. diameter) is mounted just outside this window to permit easy adjustment. The beam enters the multipass just downstream (see Ref. [2]) of the 1-in.-diameter mirror. The mirror- and incident-beam angles are adjusted so that the largest number of passes occur on the upstream side of the viewing region. This maximizes the time over which the slowly decaying excited states can be observed during their transit of the viewing region. After about 30 passes, the laser exits the multipass near its entry point.

The excited $a(1)$ level is observed through its decay fluorescence ($\lambda\approx578$ nm) to the $X(0)$, ($v''=0$) level. The methods of light collection vary and will be discussed individually with each measurement. In all cases, the light is collimated by a collection element and passes through two interference filters before being concentrated on a photomultiplier tube (PMT). Amplified signals from the PMT are sent to a photon counter (Stanford Research SR400). A PC-based running program (LABVIEW) provides a linear voltage step that controls the laser-cavity length. The laser frequency (read with a home-built wave meter) and photon count are recorded at each voltage step. We calibrate the frequency by fitting the wave-meter readings as a linear function of the

*Permanent address: Institute for Physical Research, Ashtarak-2, 378410, Armenia.

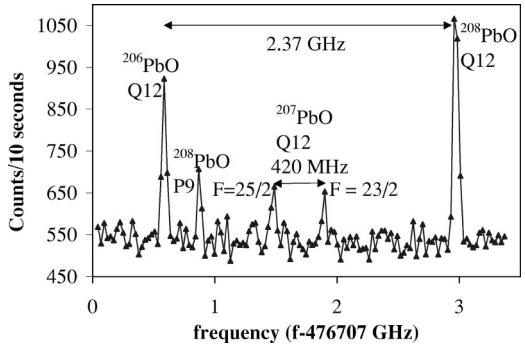

FIG. 1. A scan over the $Q12$ transition of the $X(0)(v''=2) \rightarrow a(1)(v'=3)$ transition. The ^{208}PbO and ^{206}PbO lines are prominent, with the smaller $F=25/2$ (higher frequency) and $F=23/2$ lines of ^{207}PbO split by the HFS. The ^{208}PbO P9 transition is also apparent.

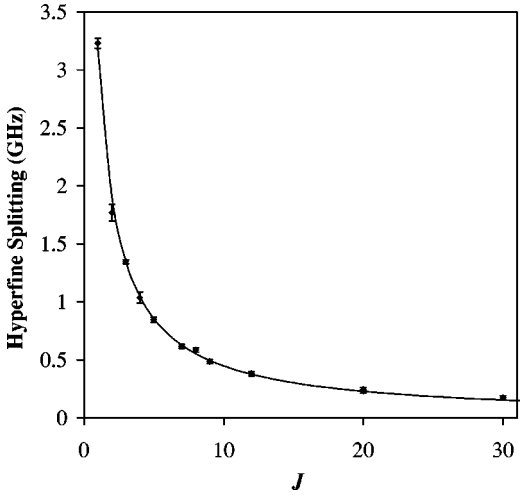

FIG. 2. The HFS of the $a(1)(v'=3)$ state of ^{207}PbO as a function of the rotational number J. The solid line is the prediction using Eqs. (1)–(3) and the best-fit value $A_{\|}=-4.11(3)$ GHz.

stepped voltage. In a 40-min scan, we can typically determine peak locations to within 200 MHz (absolute) and 20 MHz (relative).

Our first measurements using this apparatus are of isotope shifts and hyperfine structure (HFS). Here, a collimating lens ($f/3.2$) is located outside an observation window, just above the intersection of the laser multipass and the molecular beam. The laser is scanned a few gigahertz over a particular rotational transition, resulting in spectra similar to that shown in Fig. 1. Generally, four lines are evident: ^{208}Pb (nuclear spin $I=0$) is the largest, with natural abundance $N=52.3\%$; ^{206}Pb ($I=0, N=23.6\%$) is intermediate in size, and ^{207}Pb ($I=1/2, N=22.6\%$) yields two small lines of similar intensity, corresponding to the $F=J\pm 1/2$ levels that are split by the (purely magnetic) HFS in the excited state. The background is mostly due to scattered laser light. The $a(1)$ state is well described by Hund's case c [6]. For low rotational states, it is anticipated that **I** will couple to the total (electronic + rotational) angular momentum **J**; we refer to this as case c_β, in analogy with the notation for Hund's case a states. In case c_β, the HFS as a function of J will follow the form $\Delta E_{HFS}=\Delta E^{(1)}_{HFS}+\Delta E^{(2)}_{HFS}$, where the first-order splitting (diagonal in J) is [7]

$$\Delta E^{(1)}_{HFS}=A_{\|}\frac{2J+1}{2J(J+1)} \tag{1}$$

and the second-order shift (due to mixing of states with $\Delta J=\pm 1$) is [8]

$$\Delta E^{(2)}_{HFS}=-\frac{A_{\|}^2}{8B}\left[\frac{J(J+2)}{(J+1)^3}+\frac{(J+1)(J-1)}{J^3}\right]. \tag{2}$$

Here $A_{\|}$ parametrizes the HFS due to the component of the electronic angular momentum parallel to the internuclear axis, and $B=0.238\,74$ cm^{-1} is the rotational constant for the $a(1)$ ($v'=3$) level [9]. To obtain a consistent picture of the observed center of gravity of the ^{207}Pb lines as a function of J, the $F=J-1/2$ level must be at a higher energy than the $F=J+1/2$ level, i.e., $A_{\|}<0$. Figure 2 shows a plot of the observed HFS versus J; we observe no significant deviations from the anticipated scaling. The best fit value is $A_{\|}=-4.11(3)$ GHz.

The isotope shifts of ^{206}Pb and ^{207}Pb with respect to ^{208}Pb can also be extracted from these spectra. The observed shifts consist of a contribution from the nuclear reduced mass to the rovibrational-energy splittings plus an electronic contribution [10]. The rovibrational shifts for both $X(0)$ and $a(1)$ are calculated almost entirely from the precise spectroscopic data of Ref. [9]. We find that these calculated shifts depend strongly on the value of the rotational-vibrational coefficient α_e for the $a(1)$ state. This parameter has been measured twice, with values in some disagreement: Ref. [9] gives $\alpha_e=0.003\,10(131)$ cm^{-1} while Ref. [6] gives $\alpha_e=0.001\,45(20)$ cm^{-1}. We use $\alpha_e=0.0013$ cm^{-1}, which yields the most consistent values for the electronic isotope shifts from the various rotational transitions. Averaging over 15 different rotational transitions and subtracting the calculated rovibrational contributions, we find the electronic isotope shifts to be $\Delta\nu_{el}(208-207)=+368(11)$ MHz and $\Delta\nu_{el}(208-206)=+582(14)$ MHz. The electronic shift can have contributions from the field shift and the specific mass shift (the normal mass shift is much smaller than our resolution). The mass shift is proportional to the difference in the inverse of the nuclear masses involved, while the field shift depends on the density of the electronic wave function at the Pb nucleus. Hence, we can write the total electronic isotope shift as

$$\Delta\nu_{el}(a-b)=\eta[\langle r^2\rangle_a-\langle r^2\rangle_b]+\beta\left[\frac{1}{M_a}-\frac{1}{M_b}\right], \tag{3}$$

where a,b are nuclear mass numbers and $\langle r^2\rangle$ is the mean squared nuclear radius. Using the known values [11] of $[\langle r^2\rangle_a-\langle r^2\rangle_b]$ in Eq. (4) yields $\eta=6.2(10)$ GHz/fm^2 and $\beta=2.2(25)$ THz amu. Hence, the field shift between ^{208}Pb and ^{206}Pb is 0.68(11) GHz while the specific mass shift is $-0.10(12)$ GHz.

In the course of these measurements, we determine the absolute frequencies of 19 *P*-, *Q*-, and *R*-branch transitions ranging from $Q1$ through $R35$. Each $a(1)$ rotational level is split due to Ω doubling into states of opposite parity separated by a frequency $qJ(J+1)$ (where we define $q \equiv B_e - B_f$). From the frequencies of the various ^{208}Pb transitions and the precisely known spectroscopic constants of the ground state [9], we find $q = 0.000\,187(3)$ cm^{-1}. This is in excellent agreement with the less precise value reported in Ref. [9]. We also obtain a value of $B[=(B_e+B_f)/2]$, in agreement with that of Ref. [9].

Measuring the Stark effect requires observing the spectra in the presence of a uniform external electric field **E**. We have fabricated transparent electric-field plates by depositing 3.8-cm-diameter disks of indium tin oxide (ITO) on 2-in.-diameter precision quartz flats [12]. These flats, separated by 1.000(5) cm, are mounted within the vacuum chamber so that the laser multipass passes unobstructed between the plates. The fluorescent light is collected through the ITO by an aspheric lens ($f/0.78$) that rests directly on top of the upper electrode. The improved solid-angle coverage (compared with the earlier measurements) is important, since the electric field splits the lines and hence reduces their intensity. All of our Stark measurements are made on the *Q*-branch lines of ^{208}Pb, which in the absence of **E** excite only the *f* component of the Ω doublet [with parity $(-1)^{J+1}$]. For the magnitudes of *E* that we apply, the Ω-doublet states are completely mixed. The resulting Stark eigenstates have a nonvanishing expectation value in the laboratory frame of the molecular dipole moment $\boldsymbol{\mu}$, with $\boldsymbol{\mu}\cdot\mathbf{E}>0$ (<0) for the symmetric (antisymmetric) combination of the *e* and *f* states. The laser can excite transitions to either of the Stark states, with transition probability independent of the sign of $\boldsymbol{\mu}\cdot\mathbf{E}$. The energy separation of the Stark states with fixed *J* is proportional to $|m|$ (see Fig. 3).

We measure the splitting $\Delta\nu_{\pm\mu}$ between the two lines with the largest frequency separation: i.e., between the states with $|m|=J$, $\boldsymbol{\mu}\cdot\mathbf{E}>0$, and those with $|m|=J$, $\boldsymbol{\mu}\cdot\mathbf{E}<0$. For arbitrary *J*, we anticipate the relation $\Delta\nu_{\pm\mu}=2\mu_a E/[h(J+1)]$, where *h* is Planck's constant and μ_a is the molecular dipole moment of the $a(1)$ state [7]. Shifts associated with the $X(0)$ state are unimportant at the fields we apply, because the Ω-doublet splittings are much smaller than the rotational splittings that lead to the Stark effect in the ground state. This was verified explicitly by taking auxiliary data with the laser polarization $\boldsymbol{\epsilon}\perp\mathbf{E}$, but most data were taken with $\boldsymbol{\epsilon}\|\mathbf{E}$. A summary of the splittings observed on 36 independent scans over the $Q1$, $Q2$, and $Q3$ transitions is shown in Fig. 4. While the global fit is generally good, there appear to be some small systematic deviations from the expected behavior at large values of E, for both the $Q1$ and $Q2$ lines. Taking into account this small systematic effect, as well as uncertainties due to calibration and field inhomogeneity, we report a value $\mu_a = 3.27(6)$ D. We note that this value is significantly smaller than that for the $X(0)$ state: $\mu_X = 4.64(30)$ D [13].

To measure the Zeeman splitting we require a uniform magnetic field **B** over the interaction volume. The electrode assembly is removed and two coils (six turns each) are wound on the outside of our vacuum chamber. The coils are fabricated from (3/16)-in.-diameter Cu tubing and have a mean separation ≈ 2.5 in. and a mean radius ≈ 2.25 in. The coils are water cooled and can handle 300 A of current. The field at the interaction volume was determined with a Hall probe, which was calibrated against a proton nuclear magnetic resonance signal. The field is oriented along the molecular beam and varies over the interaction volume by less than 1%. Optical collection is accomplished by placing the center of the interaction region at the focus of an aluminum spherical reflector (0.75 in. focal length, 1.25 in. diameter). The reflected fluorescence is sufficiently collimated to pass through the opposing window and our two interference filters. The large magnetic fields require the PMT to be located further from the interaction region. This is accomplished by

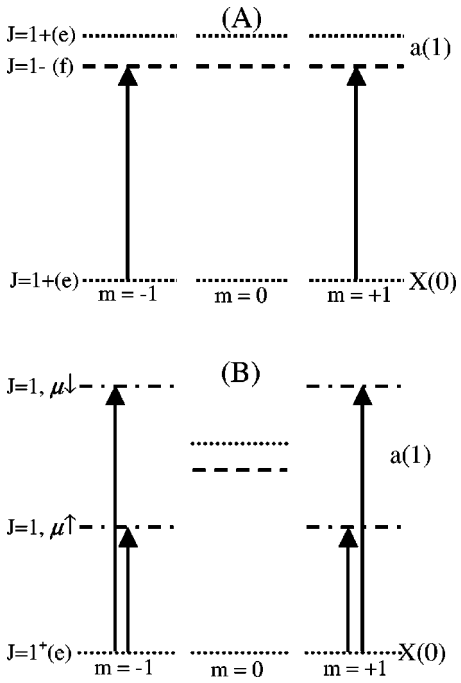

FIG. 3. Schematic description of the Stark effect on the $Q1$ line with *z*-polarized light. (a) $Q1$ line with no electric field. (b) $Q1$ line with $\mathbf{E}=E\hat{\mathbf{z}}$. Sublevels with equal values of $|m|$ remain degenerate.

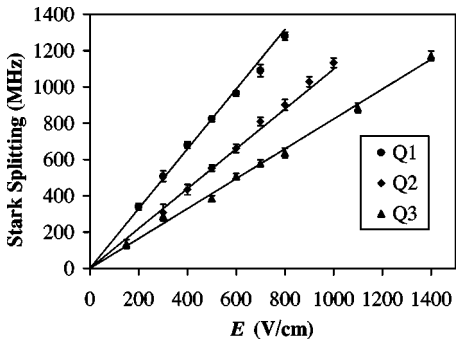

FIG. 4. The observed Stark splitting $\Delta\nu_{\pm\mu}$. The solid lines indicate the predictions for $J=1$, 2, and 3, based upon the best-fit value $\mu_a = 3.27(2)$ D.

placing a 20-in.-long, 2-in.-diameter solid plastic light guide just after the interference filters [14]. This light pipe terminates in a compound parabolic concentrator (Winston cone), which tapers down to a diameter of 1 cm just before the PMT. The laser polarization is $\boldsymbol{\epsilon} \| \mathbf{B}$ for these measurements. The splitting $\Delta \nu_{\pm m}$ is measured between the $m = J$ and $m = -J$ sublevels of the $a(1)$ state. For Hund's case c we expect this splitting to satisfy $\Delta \nu_{\pm m} = 2g\mu_B B/[h(J+1)]$, where g is the Lande g factor and μ_B is the Bohr magneton. A summary of the splittings observed on 17 independent scans across the $Q1$ and $Q2$ transitions is shown in Fig. 5. Folding in uncertainties associated with magnetic-field calibration and homogeneity, we report a value $g = 1.84(3)$.

In conclusion, we have made measurements of the HFS, molecular dipole moment, and g factor of the $a(1)$ level of PbO, and of the isotope shift of the $X(0)$-$a(1)$ transition. We have also refined the value for the Ω-doubling constant of $a(1)$. These parameters should provide valuable input to planned calculations of the sensitivity of the PbO $a(1)$ state to an electron EDM.

We thank M. Kozlov for important discussions, P. Grant for technical assistance, and E. Commins, B.C. Regan, and D. Hall for critical equipment loans. This work was supported at Amherst by NSF RUI, Grants Nos. PHY-9722611 and PHY-9987863, and at Yale by NSF, Grant No. PHY 9987846, a NIST Precision Measurement Grant, Research Corporation, the David and Lucile Packard Foundation, and the Alfred P. Sloan Foundation. S.E.M., K.A.U., and N.D.C. gratefully acknowledge NSF REU program support. S.K.P. and S.T. thank Amherst College for partial support.

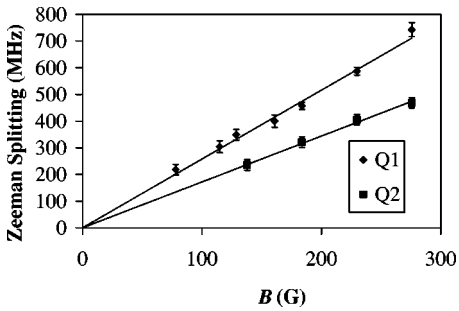

FIG. 5. The observed Zeeman splitting $\Delta \nu_{\pm m}$. The solid lines indicate the predictions for $J = 1$ and $J = 2$, based upon the best-fit value $g = 1.842(18)$.

[1] B.C. Regan, E.D. Commins, C.J. Schmidt, and D. DeMille, Phys. Rev. Lett. (to be published).
[2] D. DeMille, F. Bay, S. Bickman, D. Kawall, D. Krause, Jr., S.E. Maxwell, and L.R. Hunter, Phys. Rev. A **61**, 052507 (2000).
[3] M.G. Kozlov, Zh. Eksp. Teor. Fiz. **89**, 1933 (1985) [Sov. Phys. JETP **62,** 1114 (1985)]; M.G. Kozlov and L.N. Labzowsky, J. Phys. B **28**, 1933 (1995).
[4] M. Kozlov (private communication).
[5] A. Titov (private communication).
[6] J.M. Brom and W.H. Beattie, J. Mol. Spectrosc. **81**, 445 (1980).
[7] C.H. Townes and A.L. Schawlow, *Microwave Spectroscopy* (McGraw-Hill, New York, 1955).
[8] M. Kozlov (private communication).
[9] F. Martin *et al.*, Spectrochim. Acta **44A**, 889 (1988).
[10] H. Knöckel and E. Tiemann, Chem. Phys. Lett. **104**, 83 (1987).
[11] R.C. Thompson *et al.*, J. Phys. G **9**, 443 (1983).
[12] L.R. Hunter, D. Krause, Jr., K.E. Miller, D.J. Berkeland, and M.G. Boshier, Opt. Commun. **94**, 210 (1992).
[13] J. Hoeft *et al.*, Z. Naturforsch. A **24A**, 1222 (1969).
[14] B.C. Regan, Ph.D. thesis, University of California, Berkeley, 2001.